Aeroelastic Analysis of an Urban Air Mobility Rotor in Forward Edgewise Flight

Stephen J. Wright
Aerospace Engineer
NASA Ames Research Center
Moffett Field, CA, United States

ABSTRACT

Urban Air Mobility vehicle concepts represent a new type of vertical lift machine. From the use of multirotor configurations to the use of variable RPM for thrust control of rigid, propeller-style rotors, many of the UAM concepts observed in industry have departed significantly from traditional VTOL designs. While such novel vehicle types may provide beneficial mission capability and efficiency, they have not been as thoroughly studied as more traditional configurations, and new aeromechanics analysis must be conducted. Operating states such as low-tip-speed rotors in edgewise flight may prove to yield unusual aeroelastic behavior and must be investigated. In the present work, a rotorcraft comprehensive analysis is used to analyze the aeroelastic characteristics of a fixed-pitch, variable RPM rotor in edgewise flight. The rotor model, a three-bladed, fixed pitch propeller, was developed in a previous work. Floquet theory analysis is used to capture the periodic nature of the dynamics. Parameters such as rotor rotational speed, forward flight speed, and blade torsion stiffness are varied and their impact on performance and stability are assessed. A value of torsion stiffness is identified to yield stable flight from 0-100 kts with a wide range of RPM values. The results may be used to provide insight into the aeroelastic characteristics of certain UAM-type rotors.

NOTATION

A	rotor disk area, πR^2, ft^2
AoA	blade angle of attack, deg
b	number of blades
c	blade chord, ft
d	deflection, ft
CDO	mean drag coefficient
C_T	thrust coefficient, $T/(\rho A {V_{tip}}^2)$
EA	extensional stiffness, lb
EI_{flap}	flap stiffness, lb-ft^2
EI_{lag}	lag stiffness, lb-ft^2
GJ	torsion stiffness, lb-ft^2
R	rotor radius, ft
RPM	revolutions per minute
T	thrust, lb
UAM	urban air mobility
V	flight speed, ft/s
V_{tip}	tip speed, ΩR, ft/s
$VTOL$	vertical take-off and landing
σ	solidity, bcR/A
μ	advance ratio, V/V_{tip}
ρ	air density, slug/ft^3
Ω	rotor speed, rad/s

INTRODUCTION

In recent years, Urban Air Mobility (UAM) has garnered a great deal of interest in the aeronautics community, and the prospect of this transportation revolution has inspired investment in the design of applicable vehicles (Ref. 1). UAM missions will depend significantly on vertical take-off and landing capabilities, making lifting rotors a common element of most of the vehicle conceptual designs. However, UAM vehicle designers are often straying from traditional VTOL configurations such as helicopters and are opting for more novel vehicle systems (Ref. 2). Some of these novel configurations, such as those of the lift+cruise variety, feature lifting rotors that operate in edgewise flight during cruise. This type of operation may negatively impact vehicle performance, stability, and endurance, and further research is necessary to understand this configuration. This paper investigates stability and performance at a fundamental level using a notional, isolated rotor. Parameters such as rotor rotational speed, forward flight speed, and blade torsion stiffness were varied for the purpose of developing insight into UAM aeroelastic phenomena.

BACKGROUND

In a previous paper, a rotor model was developed to represent a generic, three-bladed, fixed-pitch rotor, representative of the scale that might be used for a UAM vehicle (Ref. 3). The rotor was loosely based on that of a quadrotor NASA UAM reference vehicle (Ref. 4). Various parameters such as airfoil,

Presented at the VFS Aeromechanics for Advanced Vertical Flight Technical Meeting, San Jose, CA, Jan 25-27, 2022.

blade torsion stiffness, and RPM, were swept and their impact on rotor performance and stability was assessed via CAMRAD II (Ref. 5), a rotorcraft comprehensive analysis code. That previous work primarily used a constant coefficient analysis for forward flight results. Floquet theory analysis, a method for analyzing stability of linear differential equations with periodic coefficients (Ref. 6), was used only minimally to provide a check on the use of the constant coefficient method. However, further analysis showed that there is a significant difference between the results of constant coefficient and Floquet analysis. These differences are highlighted in Figs. 1-5. Figure 1 is a constant coefficient, hover analysis, which reveals the unstable torsion mode. In these plots, as with most other stability plots in this paper, there are three blade modes shown, due to the use of dynamic inflow with multiblade coordinates on the three-bladed rotor. Figures 2 and 3 are the same case as Fig. 1, but with 20 kts forward flight speed. Figure 2 uses constant coefficient analysis and Fig. 3 uses Floquet analysis. Regardless of the solution method, instability is still observed in the torsion mode with a slight difference in flutter speed. Figures 4 and 5 show rotor performance at 100 kts forward flight speed for the constant coefficient analysis and the Floquet analysis respectively. It is clear that at higher speed, the difference between the two solution methods is not negligible.

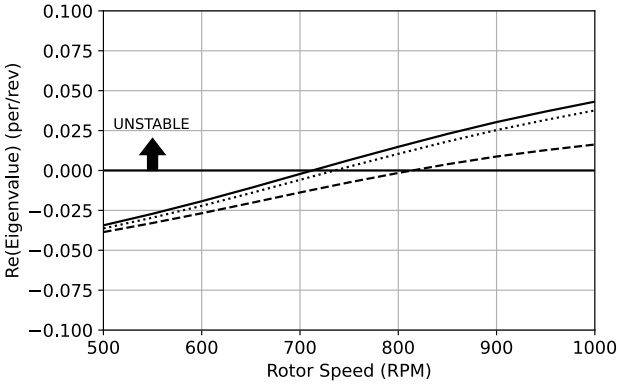

Figure 1. Stability vs rotor speed in hover, GJ = 1000 lb-ft^2, (torsion mode)

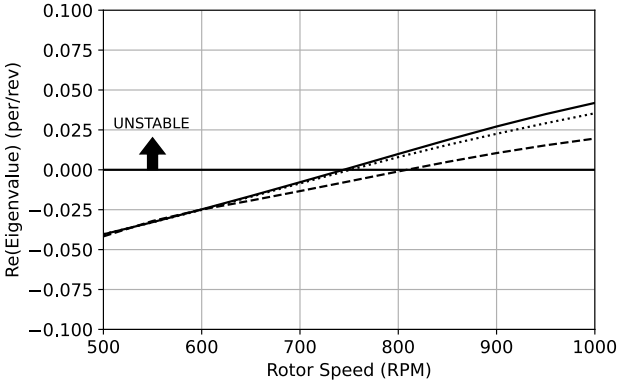

Figure 2. Stability vs rotor speed at 20 kts, GJ = 1000 lb-ft^2, constant coefficient, (torsion mode)

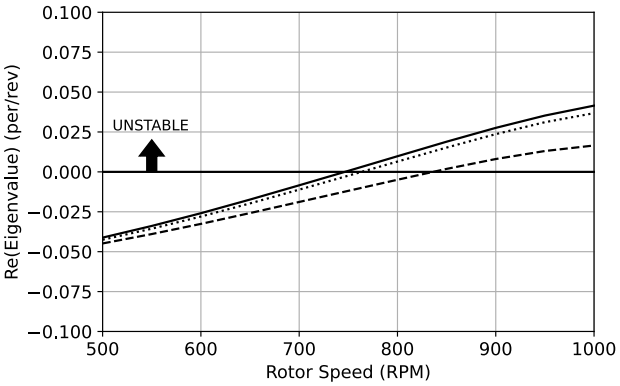

Figure 3. Stability vs rotor speed at 20 kts, GJ = 1000 lb-ft^2, Floquet theory (torsion mode)

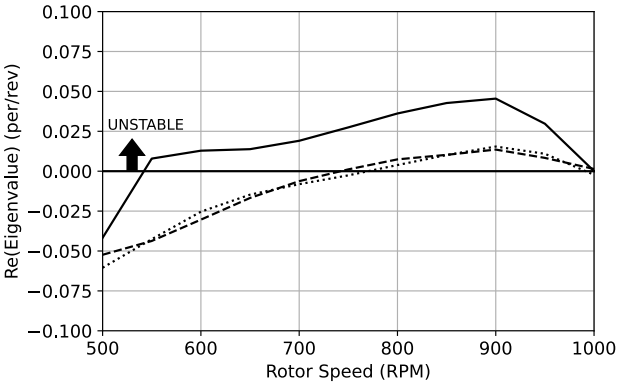

Figure 4. Stability vs rotor speed at 100 kts, GJ = 1000 lb-ft^2, constant coefficient, (torsion mode)

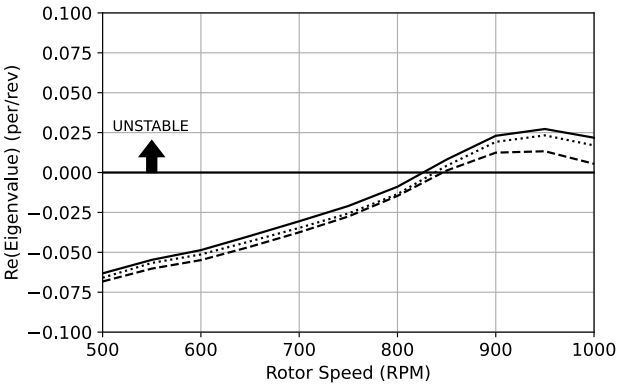

Figure 5. Stability vs rotor speed at 100 kts, GJ = 1000 lb-ft^2, Floquet theory (torsion mode)

Figure 6 plots flutter RPM vs forward flight speed for several different values of GJ and for both constant coefficient and Floquet theory analysis methods (denoted CC and FT in the legend). For GJ = 1000 and 1250 lb-ft^2, the constant coefficient analysis underpredicts flutter RPM at elevated speed. For GJ = 1500 lb-ft^2, Floquet analysis does not yield flutter beyond 40 kts, while constant coefficient analysis yields flutter at 100 kts with 900 RPM.

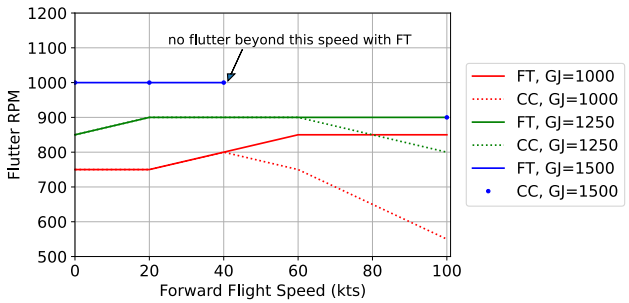

Figure 6. Flutter RPM vs forward flight speed for three GJ values, results show for both constant coefficient and Floquet theory analyses

In the present work, the previously developed rotor model was used, but forward flight was explored in greater detail via the use of Floquet analysis. Parameters such as rotor rotational speed, forward flight speed, and blade torsion stiffness were varied and their impact on performance and stability was assessed.

First, the rotor model is presented. Next, stability results are presented for the baseline value of torsion stiffness (GJ = 1000 lb-ft^2). Based on these results, an excursion of GJ values is presented, ultimately revealing a suitable GJ value (2000 lb-ft^2) for stability based on desired operating conditions. Once this GJ value is identified, envelope excursions with that value are presented. The penultimate section is devoted to an overview of rotor performance. Conclusions are summarized in the closing section of the paper.

ROTOR MODEL

Table 1, below, summarizes some of the key parameters of the rotor model, as developed in [2]. A detailed sectional design was not the source of the stiffness parameters. Rather, the stiffness values were originally chosen to give realistic values for the first flap, lag, and torsion frequencies.

Table 1. Select Rotor Model Parameters

Parameter	Value
Number of blades	3
Radius	6.94 ft
Chord	0.8721 ft
Nominal rotor speed	700 RPM
GJ	1000 lb-ft^2
EI_{lag}	5E+5 lb-ft^2
EI_{flap}	1E+5 lb-ft^2
EA	2E+7 lb
Lock number	5.0
$\sigma_{geometric}$	0.12
M_{tip} (hover)	0.4557
Twist	-13 deg

Figure 7 shows a "fan plot" of the six lowest natural frequencies of the rotor. Additionally, the first 20 n/rev frequencies are plotted. These 20 n/rev lines sufficiently cover the first six modes from the design RPM (700) to the max RPM analyzed (1000). At the nominal rotor speed of 700 RPM, the first flap, lag, and pitch frequencies are approximately 1.8/rev, 3.2/rev, and 5.2/rev, respectively.

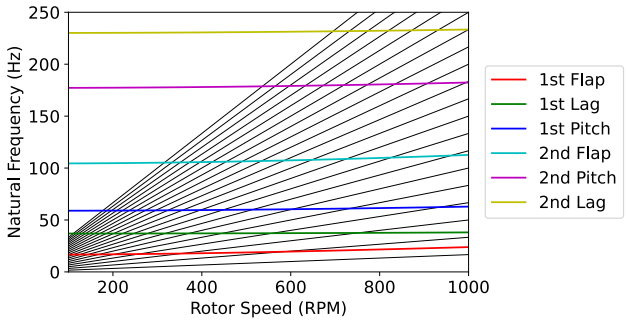

Figure 7. Natural frequency vs rotor speed in hover with baseline rotor model properties, first six modes shown, along with first 20 n/rev lines

An NACA 0012 airfoil was used. The blades have -13 deg linear twist (as specified in Table 1) and are unswept and untapered. Chordwise CG and EA are fixed at the blade quarter chord.

RESULTS WITH BASELINE GJ VALUE

Figures 8-11 plot stability vs rotor speed at various forward flight speeds (0-100 kts, with 20 kt increment). The hover case was run for the purpose of identifying the unstable modes. By gradually increasing speed, it can be determined that the unstable pitch mode in hover is the same unstable mode in the forward flight cases. As stated in a previous section, the three blade modes shown are due to the use of dynamic inflow with multiblade coordinates on the three-bladed rotor. Since the rotor's design RPM is 700, this setting of GJ is clearly insufficient. Flutter occurred for all cases within ~150 RPM of the design RPM. Since the rotor was designed to control thrust with RPM variation, this GJ is clearly unacceptable from a stability perspective.

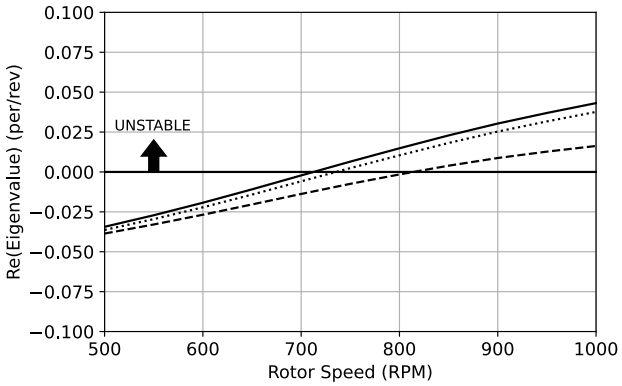

Figure 8. Stability vs rotor speed in hover, GJ = 1000 lb-ft^2 (torsion mode)

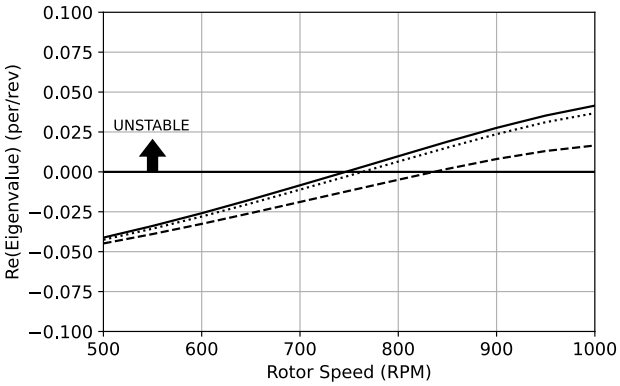

Figure 9. Stability vs rotor speed at 20 kts, GJ = 1000 lb-ft^2 (torsion mode)

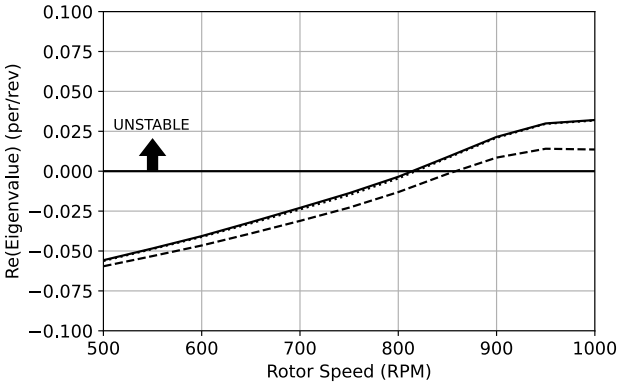

Figure 10. Stability vs rotor speed at 60 kts, GJ = 1000 lb-ft^2 (torsion mode)

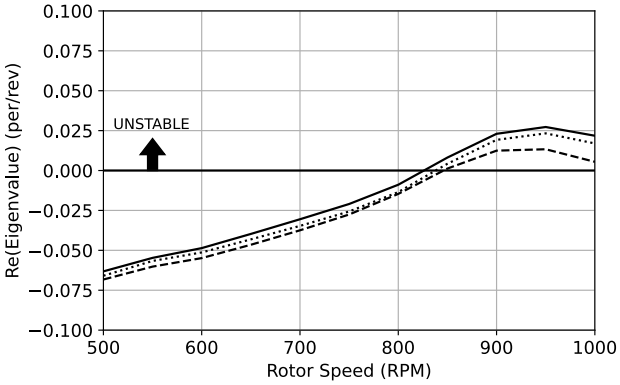

Figure 11. Stability vs rotor speed at 100 kts, GJ = 1000 lb-ft^2 (torsion mode)

FINDING MINIMUM GJ FOR 0-100 KTS AND 500-1000 RPM

In the previous section, it was shown that with GJ of 1000 lb-ft^2, the rotor flutters within ~150 RPM of the design RPM (700). For an RPM-controlled rotor, RPM settings well above and below the design speed should be usable. Following the aforementioned results based on the baseline blade torsion value (GJ = 1000 lb-ft^2), different GJ values were analyzed to determine the minimum GJ required for a forward flight speed ranging from 0-100kts with a stability boundary of at least 1000 RPM. This section highlights the results for each GJ value considered. As for previous plots of stability results, the three blade modes shown in each plot of this section are due to the use of dynamic inflow with multiblade coordinates on the three-bladed rotor.

GJ = 1250 lb-ft^2

For a blade torsion stiffness of 1250 lb-ft^2, Figs. 12-15 show stability vs rotor RPM for various speeds (0-100 kts). Increasing forward flight speed from 0 to 60 kts raises the stability boundary from ~825 RPM to approximately 900 RPM. Further increasing speed to 100 kts decreases the magnitudes of the real eigenvalue components. However, these cases flutter between 500 and 1000 RPM for all analyzed speeds.

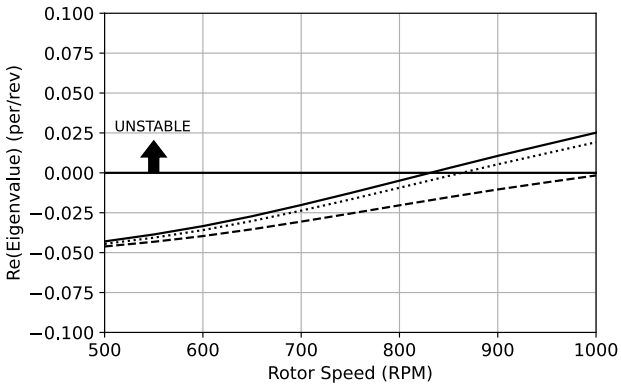

Figure 12. Stability vs rotor speed in hover, GJ = 1250 lb-ft^2 (torsion mode)

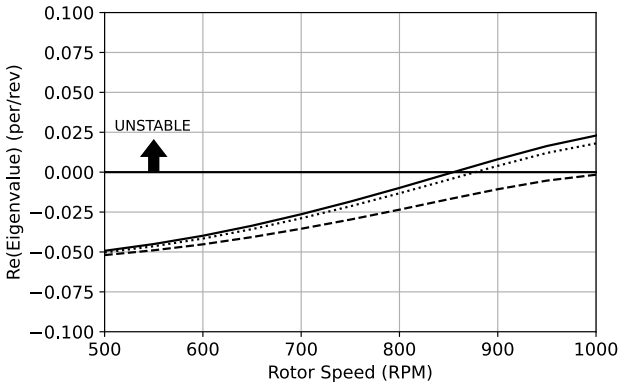

Figure 13. Stability vs rotor speed at 20 kts, GJ = 1250 lb-ft^2 (torsion mode)

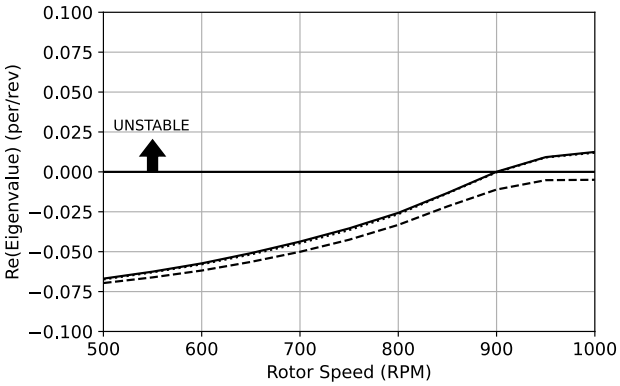

Figure 14. Stability vs rotor speed at 60 kts, GJ = 1250 lb-ft^2 (torsion mode)

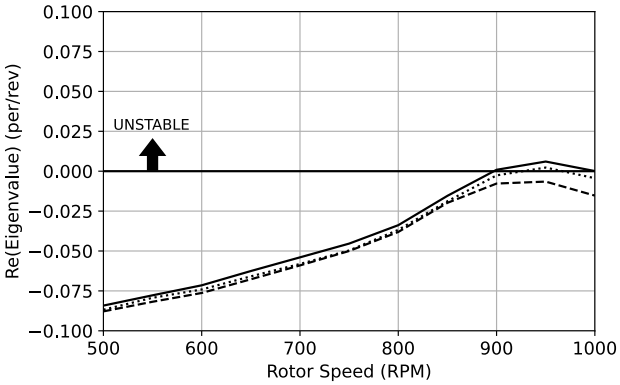

Figure 15. Stability vs rotor speed at 100 kts, GJ = 1250 lb-ft^2 (torsion mode)

GJ = 1500 lb-ft^2

Next, Figs. 16-19 show stability vs rotor RPM for various speeds (0-100 kts). For hover, and 20 kts, the rotor is unstable within the analyzed range of RPM (although the flutter RPM is quite high). For the two higher speed cases (60 and 100 kts) the rotor is stable within the range of swept RPM values. Because the rotor is unstable in hover and at low speeds, a further increase of GJ was examined.

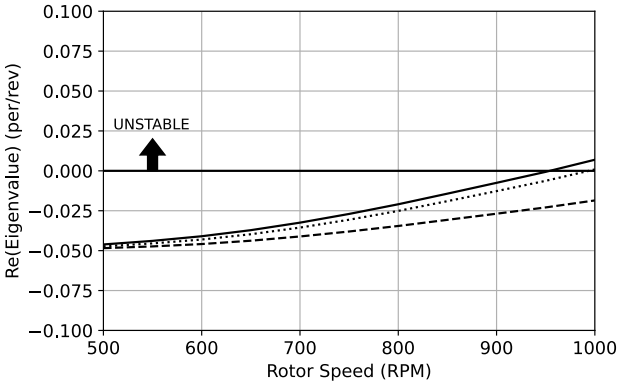

Figure 16. Stability vs rotor speed in hover, GJ = 1500 lb-ft^2 (torsion mode)

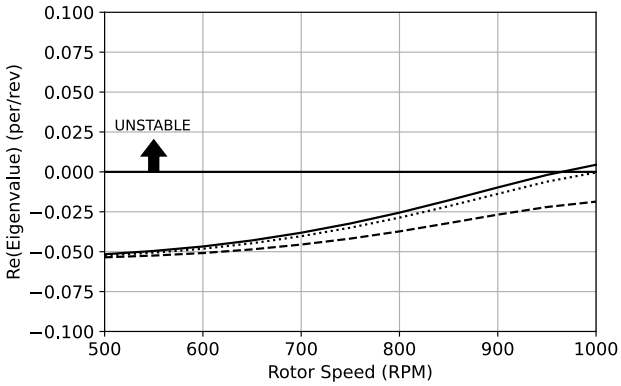

Figure 17. Stability vs rotor speed at 20 kts, GJ = 1500 lb-ft^2 (torsion mode)

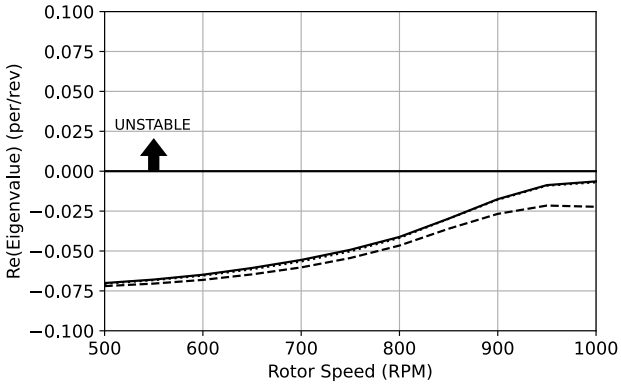

Figure 18. Stability vs rotor speed at 60 kts, GJ = 1500 lb-ft^2 (torsion mode)

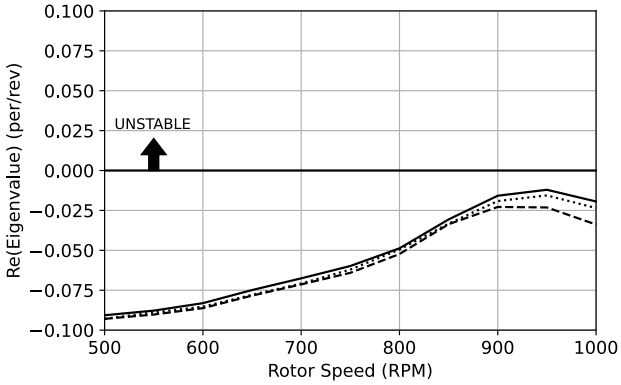

Figure 19. Stability vs rotor speed at 100 kts, GJ = 1500 lb-ft^2 (torsion mode)

GJ = 2000 lb-ft^2

Figures 20-23 show stability vs rotor RPM for various speeds (0-100 kts). As with previous sub-sections, hover was analyzed for the purpose of identifying modes. The modes plotted here are the analogues of the unstable modes from previous subsections. With GJ of 2000 lb-ft^2, the rotor is stable between 500 and 1000 RPM for all flight speeds analyzed (0-100 kts).

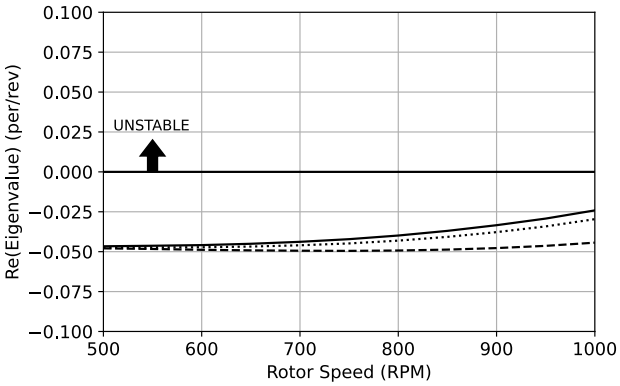

Figure 20. Stability vs rotor speed in hover, GJ = 2000 lb-ft^2 (torsion mode)

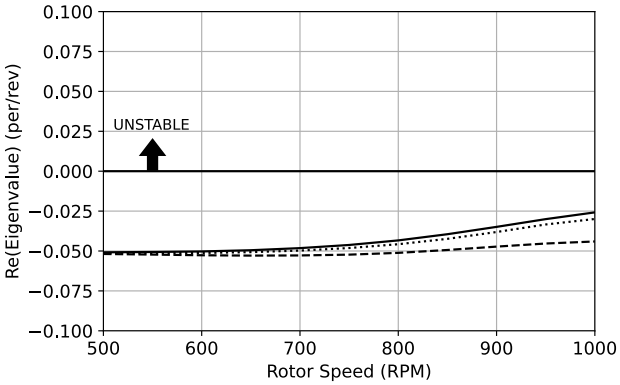

Figure 21. Stability vs rotor speed at 20 kts, GJ = 2000 lb-ft^2 (torsion mode)

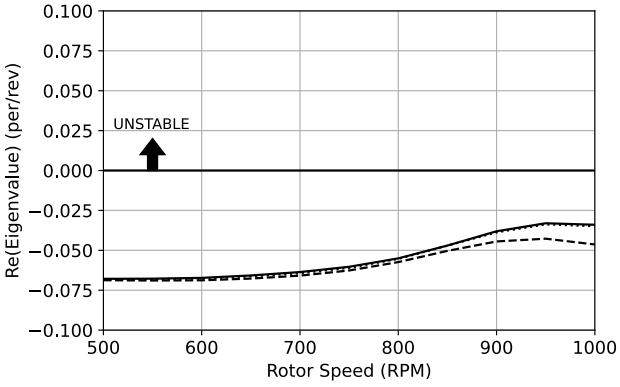

Figure 22. Stability vs rotor speed at 60 kts, GJ = 2000 lb-ft^2 (torsion mode)

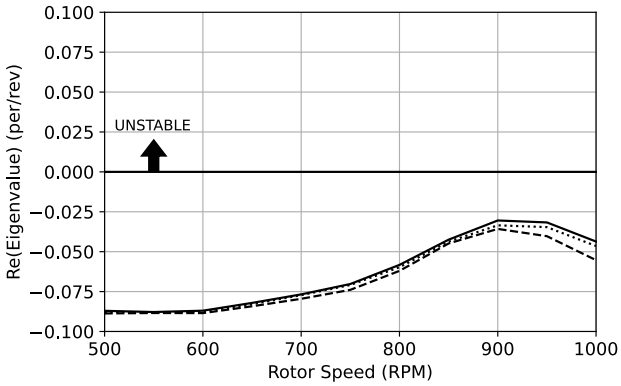

Figure 23. Stability vs rotor speed at 100 kts, GJ = 2000 lb-ft^2 (torsion mode)

For the cases presented in this section, one characteristic of interest is the increasing stability margin beyond ~900 RPM for the higher speed cases. Particularly for the 100 kt cases (Figs. 19 and 23), the magnitude of the real eigenvalue component decreases with increasing RPM (reducing the stability margin) up to ~900 RPM. Beyond 900 RPM, the stability margin improves dramatically.

To explain why stability improves beyond ~900 RPM for the higher speed cases, the analysis for which results are presented in Fig. 23 was re-run, but with elastic motion disabled in the trim solution. The results are shown in Fig. 24.

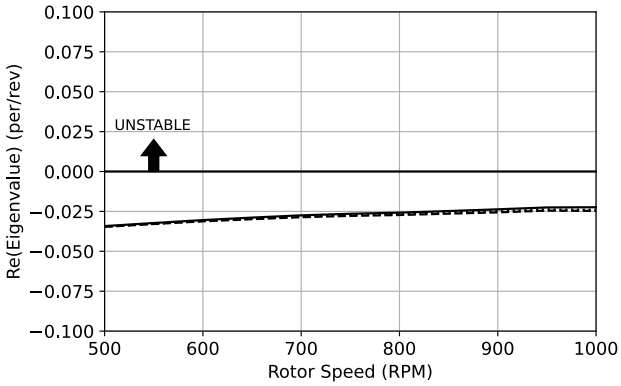

Figure 24. Stability vs rotor speed at 100 kts, GJ = 2000 lb-ft^2, no elastic motion in trim solution

Suppressing elasticity in the trim solution has a significant impact on the stability solution. To determine the nature of this impact, radial distribution of angle of attack (AoA) was investigated to determine if a significant difference in airloads with/without elasticity was causing the stability behavior. Figures 25-28 show the relationship between AoA and radial station for 0, 90, 180, and 270 deg azimuth, respectively. Results compare three different RPM values and elasticity vs no elasticity in the trim solution. Clearly, having elasticity in the trim solution does not have a major impact on the airloads, in particular, no indication of stall of the rotor blade. Elastic blade tip deflections in the flap, lag, and pitch degrees of freedom are plotted against azimuth for three different RPM values in Figs. 29-31. These figures show significant blade deflections which result in bending moments and elastic

torsion that impact the pitch-flap and pitch-lag couplings. It is likely that the elastic effects on these couplings are the cause of the stability behavior beyond 900 RPM.

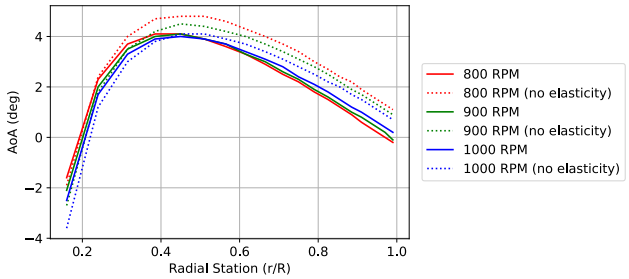

Figure 25. AoA vs radial station, PSI = 0 deg, 100 kts, results shown for three RPM, with and without elastic motion in the trim analysis

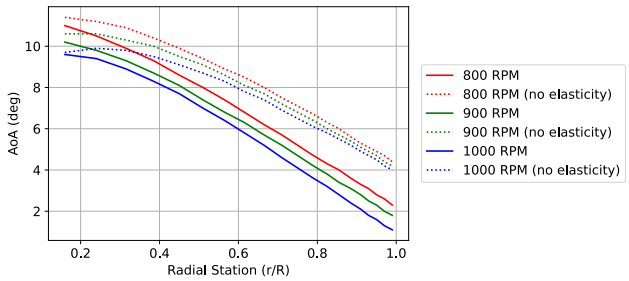

Figure 26. AoA vs radial station, PSI = 90 deg, 100 kts, results shown for three RPM, with and without elastic motion in the trim analysis

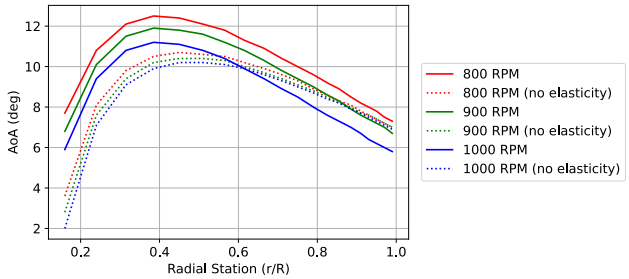

Figure 27. AoA vs radial station, PSI = 180 deg, 100 kts, results shown for three RPM, with and without elastic motion in the trim analysis

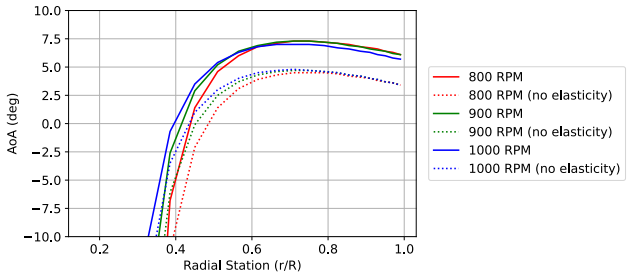

Figure 28. AoA vs radial station, PSI = 270 deg, 100 kts, results shown for three RPM, with and without elastic motion in the trim analysis

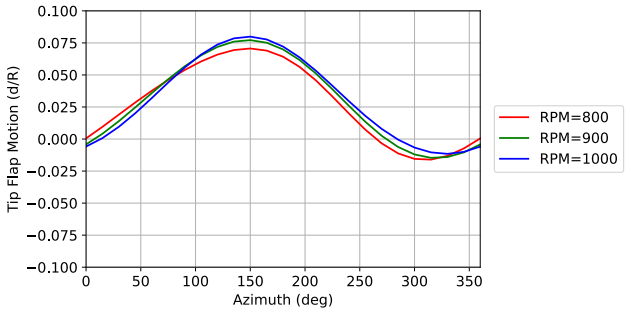

Figure 29. Flap tip motion vs azimuth, 100 kts, results shown for three different RPM values

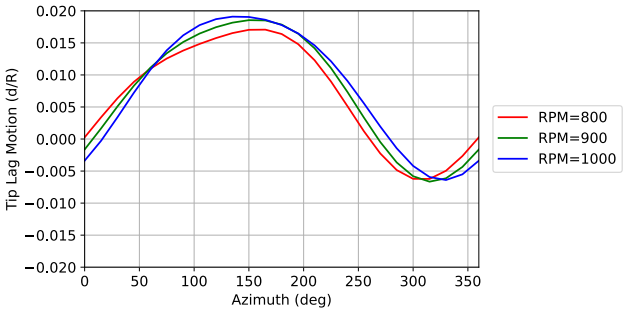

Figure 30. Lag tip motion vs azimuth, 100 kts, results shown for three different RPM values

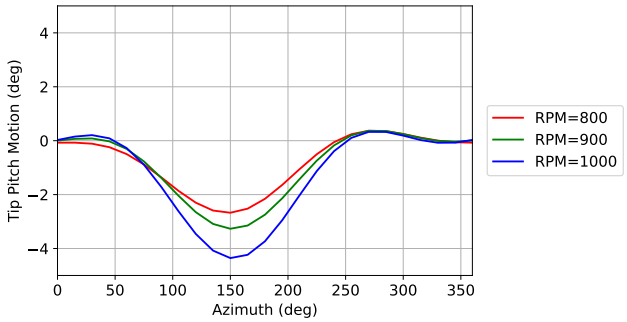

Figure 31. Tip pitch motion vs azimuth, 100 kts, results shown for three different RPM values

ENVELOPE EXPLORATION

In the previous section, results were presented for a series of RPM sweeps with GJ = 2000 lb-ft^2. In the present section, results are presented for a wider range of cases with this same GJ setting. As before, when three blade modes are shown, this is due to the use of dynamic inflow with multiblade coordinates on the three-bladed rotor.

Flight Speed Sweeps – Fixed RPM

Figures 25-27 are plots of stability vs flight speed at various rotor speed operating conditions. Minimally-damped modes are plotted. Flutter is not encountered in any of the three sweeps.

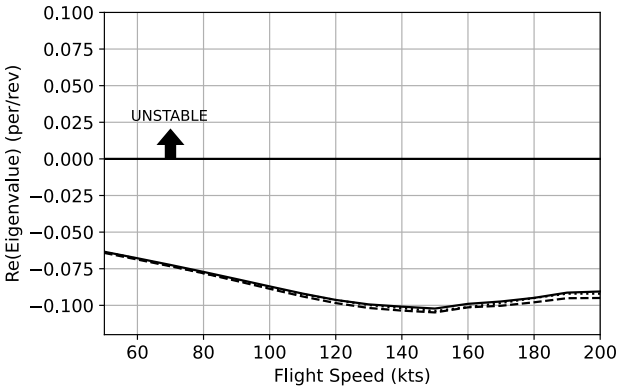

Figure 25. Stability vs flight speed at 500 RPM, GJ = 2000 lb-ft^2

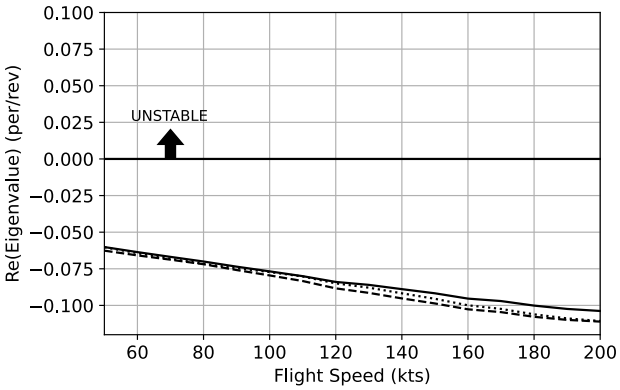

Figure 26. Stability vs flight speed at 700 RPM, GJ = 2000 lb-ft^2

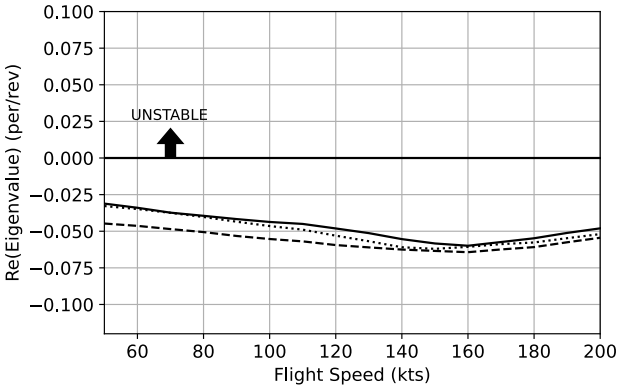

Figure 27. Stability vs flight speed at 1000 RPM, GJ = 2000 lb-ft^2

RPM Sweeps – Fixed Flight Speed

Figures 28-29 are plots of stability vs rotor speed for two elevated forward flight speed conditions. Flutter does not occur for either sweep.

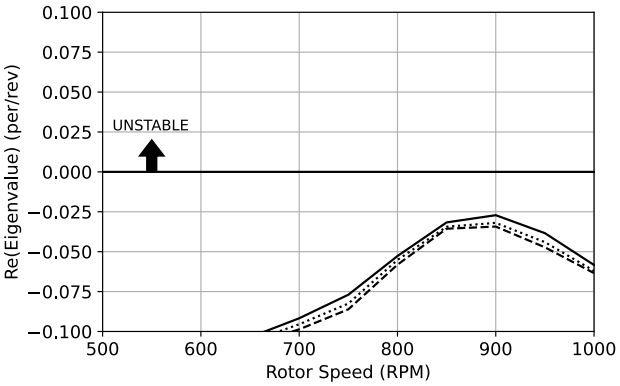

Figure 28. Stability vs rotor speed at 150 kts, GJ = 2000 lb-ft^2

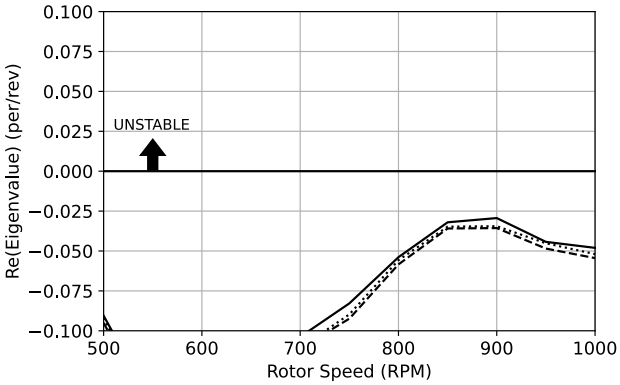

Figure 29. Stability vs rotor speed at 200 kts, GJ = 2000 lb-ft^2

PERFORMANCE EXPLORATION

Figures 30 and 31 show two key metrics of rotor performance with GJ = 2000 lb-ft^2. As with the stability analysis, these forward flight cases were run with fixed pitch blades and 0-degree shaft angle. Figure 30 shows C_T/σ vs advance ratio (μ) for three different RPM values (speed is swept). Figure 29 shows mean drag coefficient (CDO) vs μ for the same three RPM values (speed is swept). CDO is defined per equation 1 where F*(μ)* accounts for the increase in mean dynamic pressure of blade section with speed (Ref. 7).

$$CDO = \frac{8CP_o/\sigma}{F(\mu)} \qquad [1]$$

Assuming a doubling of CDO indicates substantial stall on the rotor disk, approximate stall advance ratios can be inferred from Fig. 31. These stalling μ values are tabulated in Table 2.

Figure 32 is a plot of blade tip pitch motion vs advance ratio (the red line indicates 0 deg pitch). Blade tip pitch is negative for all cases. For 700 and 1000 RPM, the tip pitch decreases with advance ratio throughout the entirety of the sweep. The 1000 RPM case in particular shows a very dramatic increase in nose-down pitch beyond about 0.2 advance ratio.

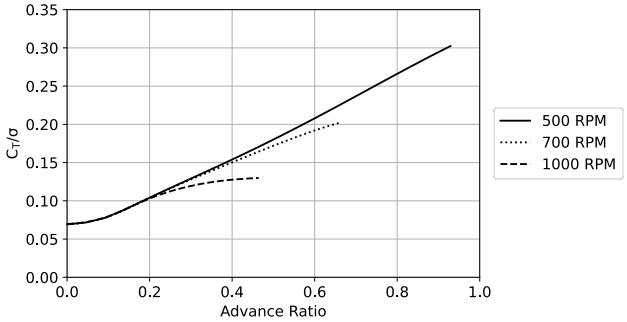

Figure 30. C_T/σ vs advance ratio (flight speed swept) for three rotor speeds, GJ = 2000 lb-ft^2

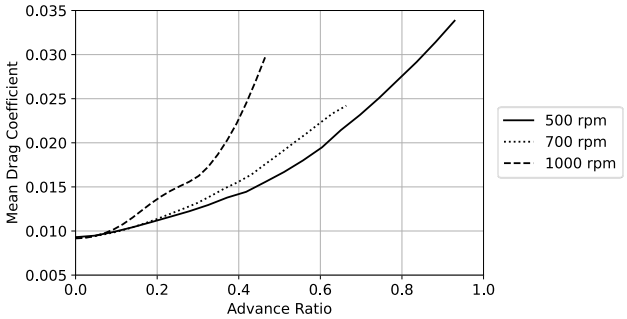

Figure 31. CDO vs advance ratio (flight speed swept 0 to 200 knots) for three rotor speeds, GJ = 2000 lb-ft^2

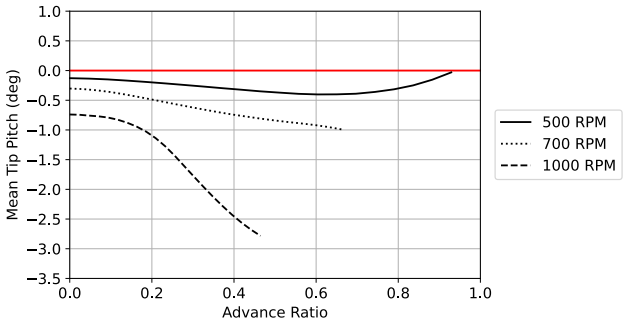

Figure 32. Mean of blade tip pitch vs advance ratio (flight speed swept 0 to 200 knots) for three rotor speeds, GJ = 2000 lb-ft^2

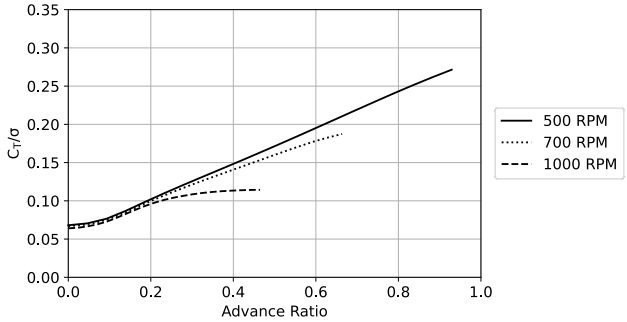

Figure 33. C_T/σ vs advance ratio (flight speed swept 0 to 200 knots) for three rotor speeds, GJ = 1000 lb-ft^2

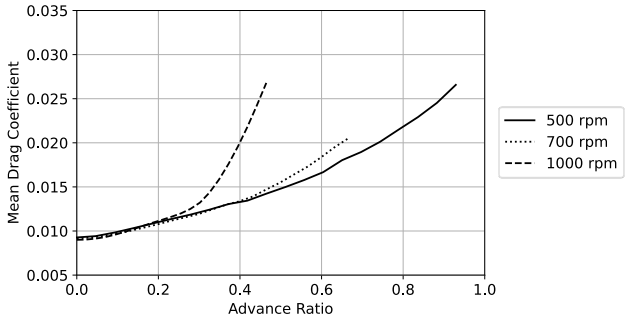

Figure 34. CDO vs advance ratio (flight speed swept 0 to 200 knots) for three rotor speeds, GJ = 1000 lb-ft^2

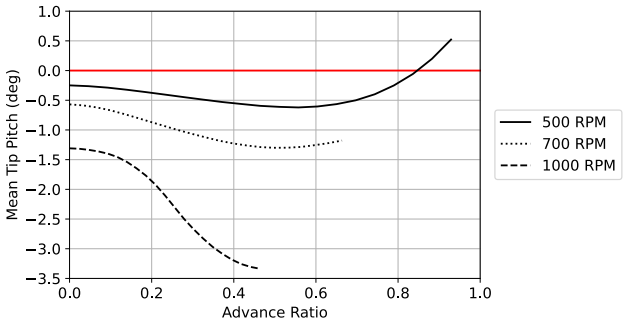

Figure 35. Mean blade tip pitch vs advance ratio (flight speed swept 0 to 200 knots) for three rotor speeds, GJ = 1000 lb-ft^2

Figure 33 shows C_T/σ vs μ for three different RPM values (speed is swept). Figure 32 shows CDO vs μ for the same three RPM values (speed is swept). Assuming a doubling of CDO indicates substantial stall on the rotor disk, approximate stall advance ratios can be inferred from Fig. 34 (values tabulated in Table 2).

Figure 35 is a plot of blade tip pitch motion vs advance ratio. As can be seen, blade tip pitch is negative for all cases *except* for 500 RPM with μ in excess of 0.8. The 1000 RPM case shows a very dramatic decrease in tip pitch beyond μ of about 0.1.

Table 2 summarizes the approximate stalling advance ratios and corresponding speeds for the three RPM settings (500, 700, and 1000 RPM) and for the two values of GJ (1000 and 2000 lb-ft^2).

Table 2. Approximate Stalling Advance Ratios

GJ = 2000 lb-ft^2			GJ = 1000 lb-ft^2		
RPM	μ	Speed (kts)	RPM	μ	Speed (kts)
500	.557	120	500	.697	150
700	.498	150	700	.597	180
1000	.348	150	1000	.372	160

For GJ = 2000 lb-ft^2, increasing the operating RPM reduces the stalling advance ratio. Increasing from 500 RPM to 700 RPM increases the stalling speed (but increasing from 700 to 1000 RPM does not). Additionally, comparing the stall RPMs

from GJ = 2000 lb-ft^2 and 1000 lb-ft^2, it can be inferred that the softer-in-torsion rotor can achieve higher advance ratios and speeds than the stiffer blade (the difference is quite pronounced at 500 and 700 RPM).

CONCLUSIONS

This work demonstrates several points of interest, as well as some general trends that apply to fixed pitch, variable RPM rotors of this type.

1. For forward flight, it is essential to use Floquet theory analysis. The constant coefficient analysis was shown to find a different stability boundary; Floquet theory captures the periodicity of the problem and is necessary for more accurate results.
2. Increasing GJ increases the flutter RPM (or eliminates flutter altogether). This was demonstrated by incrementally increasing GJ until flutter was eliminated from 0 to 200 kts with 500-1000 RPM.
3. Increasing RPM reduces the stalling advance ratio; however, in certain RPM ranges, an increase in RPM may yield a higher stalling speed.
4. Increasing GJ results in lower stalling advance ratio and lower stalling speed. This leads to the significant conclusion that there is an inherent trade between stability and performance. Specifically, maximizing flutter RPM trades with forward flight speed.

Author contact: Stephen Wright stephen.j.wright@nasa.gov

ACKNOWLEDGMENTS

I thank my colleagues within the NASA Ames Rotorcraft Aeromechanics Branch for their support. Particular gratitude goes to Wayne Johnson for his insight regarding rotorcraft theory and for his guidance with his CAMRAD II program. I also thank William Warmbrodt for his mentorship; one could not ask for a better supervisor.

REFERENCES

1. Dudley, M.R., "Second Annual Transformative Vertical Flight Concepts Workshop. Enabling New Flight Concepts Through Novel Propulsion and Energy Architectures," NASA CR 2016-219141, August 2015.

2. Antcliff, K.R., Moore, M.D., and Goodrich, K.H., "Silicon Valley as an Early Adopter for On-Demand Civil VTOL Operations," AIAA Paper No. 2016-3466, June 2016.

3. Wright, S.J., "Fundamental Aeroelastic Analysis of an Urban Air Mobility Rotor," VFS Autonomous VTOL Technical Meeting, (Virtual), January 2021.

4. Silva, C., Johnson, W., and Solis, E., "Concept Vehicles for VTOL Air Tax Operations," AHS Technical Meeting on Aeromechanics Design for Vertical Lift, Holiday Inn at Fisherman's Wharf, San Francisco, CA, January 16-18, 2018.

5. Johnson, W., "Rotorcraft Aeromechanics Applications of a Comprehensive Analysis," HeliJapan 1998: AHS International Meeting on Rotorcraft Technology and Disaster Relief, Gifu, Japan, April 1998.

6. Johnson, W., *Rotorcraft Aeromechanics*, Cambridge University Press, New York, NY, 2013, pp. 568-572.

7. Johnson, W., "NDARC. NASA Design and Analysis of Rotorcraft," NASA TP 2015-218751, April 2015.